

Incident light dependence for photocatalytic degradation of acetaldehyde and acetic acid on S-doped and N-doped TiO₂ photocatalysts

Kazumoto Nishijima ^a, Bunsho Ohtani ^b, Xiaoli Yan ^b, Taka-aki Kamai ^a, Tetsuo Chiyoya ^a, Toshiaki Tsubota ^a, Naoya Murakami ^a, Teruhisa Ohno ^{a,*}

^a *Department of Materials Science, Faculty of Engineering, Kyushu Institute of Technology, 1-1 Sensuicho, Tobata, Kitakyushu 804-8550, Japan*

^b *Catalysis Research Center, Hokkaido University, Kita-ku N21W10, Sapporo 001-0021, Japan*

Abstract

We have synthesized S (S⁴⁺)-doped and N (N³⁻)-doped TiO₂ photocatalysts. S-doped and N-doped TiO₂ loaded with Fe₂O₃ nano- particles have also been prepared. These photocatalysts showed activity under a wide range of wavelengths of irradiation. Action spectra of photochemical reaction rate as a function of the incident light wavelength for oxidation of acetic acid on S-doped TiO₂ was studied. The photocatalytic activities of S-doped and N-doped TiO₂ photocatalysts loaded with Fe₂O₃ nanoparticles for oxidation of acetic acid in aqueous phase and acetaldehyde in gas phase are markedly improved compared to those of doped TiO₂ without loading of Fe₂O₃ nanoparticles under a wide range of incident light wavelengths. The optimum amount of Fe₂O₃ nanoparticles loaded on S-doped TiO₂ particles was different from that on N-doped TiO₂ for oxidation of organic compounds. The relationship between reaction rate of photocatalytic oxidation of acetaldehyde on doped TiO₂ loaded with Fe₂O₃ nanoparticles and amount of Fe₂O₃ nanoparticles is discussed.

Keywords: S-doped TiO₂; N-doped TiO₂; Loading of Fe₂O₃ nanoparticle; Degradation of acetaldehyde; Improvement of charge separation

1. Introduction

Environmental pollution and destruction on a global scale are issues of increasing concern in today's society. There is a need for effective catalysts for degradation of pollutants. In recent years there has been much interest in the use of semiconductors as photocatalysts to initiate photocatalytic reactions at their interfaces [1]. Metal oxide semiconductor powders that show activity when irradiated with ultraviolet (UV) light have been used as photocatalysts for degradation of pollutants. TiO₂ has been widely used a catalyst because of its merits, including optical and electronic properties, low cost, high level of photocatalytic activity, chemical stability and non-toxicity [2].

Since the discovery of photoelectrochemical splitting of water on titanium dioxide (TiO₂) electrodes [3], semiconductor-based photocatalysis has received much attention [1,4–16]. Most of these investigations have been carried out under UV light because a TiO₂ photocatalyst shows relatively high levels of activity and chemical stability under UV light, which exceed the band-gap energy of 3.0 or 3.2 eV in the rutile or anatase crystalline phase, respectively. Although TiO₂, one of the most promising photocatalysts, is now used in various practical applications [1,11], only a small UV fraction of solar light, about 2–3%, can be utilized because of its large band gap of 3.2 eV.

The development of photocatalysts that show a high level of activity under visible light irradiation is needed in order to utilize sunlight or rays from artificial sources more effectively in photocatalytic reactions. In the past, transition metal cations have been used as dopants to red-shift the absorption edge of TiO₂ and SrTiO₃ to a visible light region [17–29]. For this purpose, reduced forms of TiO_x photocatalysts [30,31] have been also investigated.

Treatment of TiO₂ powder with hydrogen peroxide [32] or chelating agents [33] allows some photocatalytic reactions to proceed under visible light. However, most of these catalysts do not show long-term stability or do not have sufficiently high levels of activity for a wide range of applications. Asahi et al. [34] reported that N-doped TiO₂ shows photoabsorption at wavelengths longer than 400 nm. It has also been reported that N-doped TiO₂ has photocatalytic activity under visible light. Recently, Umebayashi et al. have succeeded in synthesizing TiO₂ doped with S anions [35]. Kahn et al. [36] reported that C-doped TiO₂ was obtained as a result of a chemical modification of TiO₂ by controlled combustion of titanium metal in a natural gas flame. These compounds absorb visible light. These findings are supported by the results of theoretical calculations using full-potential linearized

augmented plane wave formalism (F-LAPW method). However, the absorption spectra of these compounds in the visible region are relatively small. It should also be noted that dopants such as N and C are incorporated as anions and replaced by oxygen in the lattice of TiO₂. Other techniques for synthesizing TiO₂ photocatalysts showing relatively high levels of activity under visible light have also been developed recently [37,38]. We have also developed and reported the synthesis of S-cation-doped TiO₂ having anatase or rutile phase and Fe₂O₃ nanoparticles loaded on the surface of S-doped and N-doped TiO₂ [39–42].

We have succeeded in preparing S-doped and N-doped TiO₂ photocatalysts loaded with Fe₂O₃ nanoparticles having an anatase phase in order to enhance the charge separation between electrons and holes, resulting in improvement in photocatalytic activity for oxidation of organic compounds under the condition of visible light irradiation. These activity enhancements were improved by reduction and air oxidation of the doped TiO₂ powders loaded with Fe₂O₃ nanoparticles.

In the present paper, we report action spectra, i.e., plots of photochemical reaction rate or yield per unit number of incident photons as a function of wavelength. Studies have been carried out on photodegradation of methylene blue (MB) [43–45] as a representative dye for systems of activity evaluation by comparison with the results of tests on decomposition of acetic acid (AcOH) in its aerated suspension system. In addition, the reaction mechanism for degradation of acetic acid on doped TiO₂ loaded with or without Fe₂O₃ nanoparticles in gas phase has been studied. It has also been shown that the reaction mechanism of photocatalytic oxidation of acetaldehyde on doped TiO₂ loaded with Fe₂O₃ nanoparticles changed with change in the amount of Fe₂O₃ nanoparticles.

2. Experimental

2.1. Materials and instruments

Titanium dioxide (TiO₂) powder having an anatase phase was obtained from Ishihara Sangyo (ST-01). P-25 having a mixture of anatase and rutile phases was obtained from Japan Aerosil. The relative surface areas of ST-01 and P-25 were 285.3 and 49.2 m²/g, respectively. The content of anatase phase of P-25 is 73.5%. Acetaldehyde, acetic acid, and FeCl₃ were obtained from Wako Pure Chemical Industry. Thiourea and urea were obtained from Tokyo Chemical Industry Co. Ltd. Other chemicals were obtained from commercial sources as guaranteed reagents and were used without further purification. The crystal structures of TiO₂ powders were determined from X-ray diffraction (XRD) patterns measured with an X-ray diffractometer (Philips, X'Pert-MRD) with a Cu target Ka-ray ($k = 1.5405 \text{ \AA}$). The relative surface areas of the powders were determined by using a surface area analyzer (Micromeritics, FlowSorb II 2300). The absorption and diffuse reflection spectra were measured using a Shimadzu UV-2500PC spectrophotometer. X-ray photoelectron spectra (XPS) of the TiO₂ powders were measured using a JEOL JPS90SX photoelectron spectrometer with an Al Ka source (1486.6 eV). The shift of binding energy due to relative surface charging was corrected using the C 1s level at 285 eV as an internal standard. The XPS peaks were assumed to have Gaussian line shapes and were resolved into components by a non-linear least-squares procedure after proper subtraction of the baseline. ESR spectra were obtained on a JEOL JES-ME3 X-band spectrometer equipped with a 100 kHz field modulation unit; a standard MgO/Mn²⁺ sample calibrated with an NMR magnetometer was employed for calibration of the magnetic field. DRIFTS (diffuse reflectance infrared Fourier transform spectroscopy) was used to analyze the nature of the adsorbed species on the photocatalyst. The system consisted of an FTIR spectrometer (Jasco FT/IR-4200) equipped with a DRIFTS cell (Jasco DR-81 Diffuse Reflectance Attachment).

2.2. Preparation of S-doped and N-doped TiO₂ powders loaded with Fe₂O₃ nanoparticles

S-doped and N-doped TiO₂ powders as starting materials were synthesized by previously reported methods [39–42,46]. An appropriate amount of FeCl₃ was dissolved in deionized water (300 ml). Three g of the doped TiO₂ powder was suspended in a FeCl₃ aqueous solution, and the solution was stirred vigorously for 2 h. After filtration of the solution, the amount of Fe³⁺ ions that remained in the solution was determined by UV absorption spectra to estimate the amount of Fe₂O₃ loaded on the doped TiO₂ powder. Determination of Fe³⁺ ions in aqueous solution was measured by absorption of colored Fe³⁺ aqueous solution by HCl. The residue was washed with deionized water several times until pH of the filtrate was neutralized. The powders were dried under reduced pressure at 60 °C for 12 h. Detailed conditions for preparation are shown in Table 1. In order to analyze the chemical states of Fe₂O₃ loaded on the doped TiO₂ during photoirradiation, ESR spectra of the doped TiO₂ particles loaded with Fe₂O₃ were observed under reduced pressure and an aerated condition at 77 K. A 350-W high-pressure mercury lamp (WACOM Co. Ltd., BMI-350DI) was used as an irradiation light source. After photoirradiation, the powder was

exposed to air and analyzed by ESR spectroscopy again.

2.3. Monochromatic photoirradiation for oxidation of acetic acid on S-doped TiO₂

Photocatalytic decomposition of acetic acid (Wako Pure Chemical, 0.05 mmol dm⁻³) in an aerated aqueous solution (Milli-Q water prepared with Yamato-Millipore WQ501; 3.0 cm³, adjusted to pH 3 by addition of hydrochloric acid) containing 30 mg of a photocatalyst was studied under monochromatic irradiation under air. The suspensions were stirred in the dark for 2 h to reach adsorption equilibrium and were then subjected to monochromatic irradiation for 30 min in the range of 290–680 nm using a diffraction grating-type illuminator (Jasco CRM-FD) equipped with a 300-W xenon lamp (Hamamatsu Photonics C2578-02). The intensity of irradiation, measured by a Molectron PM5200 laser power meter, was in the range of 1.98–6.52 · 10⁻⁸ einstein s⁻¹. The molar amounts of liberated carbon dioxide (CO₂) as a result of decomposition of acetic acid were measured by a gas chromatograph (Shimadzu GC-14B) equipped with a flame ionization detector (FID) and a methanizer (Shimadzu MTN-1). The irradiation was continued until an almost linear increase in the CO₂ amount was observed. The apparent quantum yield (U_{app}) was calculated as a ratio of the molar rate of the generation of CO₂ to the flux of incident photons.

2.4. Photocatalytic degradation of acetaldehyde, formic acid, or acetic acid on the doped TiO₂ in gas phase

The photocatalytic activities of S-doped and N-doped TiO₂ loaded with Fe₂O₃ nanoparticles were evaluated by measuring the change in concentration of acetaldehyde and evolved CO₂ as a function of irradiation time. A Tedlar bag (AS ONE Co. Ltd.) was used as the photo-reactor vessel with a volume of 125 cm³. One hundred milligram of the TiO₂ powder was spread evenly on the bottom of a glass dish (area: 9.6 cm² = irradiation area), and this was placed in the reaction vessel described above.

23

Five hundred ppmv of acetaldehyde, formic acid, or acetic acid was prepared in the vessel by injection of saturated gaseous acetaldehyde. The irradiations were conducted at room temperature after equilibrium between the gaseous and adsorbed acetaldehyde had been reached (as ascertained by monitoring the concentration chromatographically about every 30 min). A 500-W Xe lamp (USHIO Co. Ltd., SX-UI501XQ) was used as a light source. To limit the irradiation wavelengths, the light beam was passed through a UV-35, L-42 or Y-47 filter (Kenko Co.) to cut off wavelengths shorter than 350, 420 or 470 nm, respectively. Fine stainless meshes were used as neutral density filters to adjust the irradiation intensity (12.7 mW cm⁻²). After starting the irradiation, the decrease in acetaldehyde concentration was measured using a gas chromatograph (Shimadzu Model GC-8A, FID detector) equipped with an FEG-20 M 20% Celite 545 packed glass column using CR-8A CHROMATOPAC for data processing. At the same time, the amount of gaseous carbon dioxide evolved was analyzed using a gas chromatograph (Shimadzu Model GC-9A, FID detector) equipped with a TCP 20% Uniport R packed column and a methanizer (GL Sciences, MT-221) operated at a temperature of 375 °C and using CR-8A CHROMATOPAC for data processing.

3. Results and discussion

3.1. Absorption ESR and XRD spectra of S-doped and N-doped TiO₂ loaded with Fe³⁺ compounds

Fig. 1 shows absorption spectra of S-doped and N-doped TiO₂ loaded with Fe³⁺ compounds. The absorption spectra of the Fe³⁺ compounds loaded only on the surface of doped TiO₂ particles in the visible region gradually changed with increase in the amount of Fe³⁺ compounds as shown in Fig. 1. The change in absorbance of S-doped and N-doped TiO₂ loaded with Fe³⁺ compounds was derived from Fe³⁺ compounds on doped TiO₂, which is thought to show absorbance in the visible light region.

Fig. 2 shows ESR spectra of N-doped TiO₂ adsorbed with Fe³⁺ compounds under reduced pressure. A broad peak at 4.4 assigned to Fe³⁺ species was observed. The peak completely disappeared under the condition of photoirradiation using a high-pressure mercury lamp (350 W; 18.5 mW/cm²) for 30 min. These results suggested that Fe³⁺ ions were efficiently reduced by photoexcited electrons to generate Fe²⁺ ions that are not detected by ESR measurement under reduced pressure. The results of ESR measurements in the case of S-doped TiO₂ adsorbed with Fe³⁺ compounds were similar to those in the case of N-doped TiO₂ with Fe³⁺ ions. Fig. 3 shows XRD spectra of S-doped TiO₂ loaded with Fe³⁺ compounds. A small peak at 35.8°, which was assigned to c-Fe₂O₃, was observed [47–49]. In the case of N-doped TiO₂ loaded with Fe³⁺ compounds, a peak assigned to c-Fe₂O₃ was too weak to observe. These results indicate that photoexcited electrons

were efficiently trapped by oxygen through Fe₂O₃ nanoparticles loaded on the surface of the doped TiO₂ photocatalysts resulting in enhanced charge separation as discussed later.

3.2. VIS light activity of S-doped TiO₂ loaded with Fe₂O₃ nanoparticles under polychromatic irradiation

In order to elucidate the effect of Fe₂O₃ modification on the surface of S-doped TiO₂ for improvement of VIS-light activity, the reaction rates of AcOH decomposition in aqueous phase on several kinds of TiO₂ photocatalysts under polychromatic visible light irradiation ($\lambda > 430$ nm) were measured. The results are shown in Fig. 4. The results indicate that S-doped TiO₂ loaded with Fe₂O₃ nanoparticles (1.0 wt%) has the strongest VIS response among the photocatalysts examined, and the reaction rate is almost 2.8-times higher than that of S-doped TiO₂ without loading of Fe₂O₃ nanoparticles.

3.3. Action spectra measurement of AcOH decomposition on S-doped TiO₂ loaded with Fe₂O₃ nanoparticles

Fig. 5 shows the action spectra of P-25, pure S-doped TiO₂ and S-doped TiO₂ loaded with Fe₂O₃ nanoparticles for oxidative decomposition of AcOH in an aerated aqueous solution. Since the stoichiometry in this photocatalytic reaction system is known to be $\text{CH}_3\text{COOH} + 2\text{O}_2 = 2\text{CO}_2 + 2\text{H}_2\text{O}$, we ignored a possible radical chain mechanism and assumed eight holes and electrons are required when U_{app} was calculated. After manipulation, the final calculation formula of U_{app} is shown in the following equation:

$$\Phi_{\text{app}} = \frac{r \cdot a}{\lambda \cdot I}, \quad (1)$$

TiO₂ and pure TiO₂ (ST-01, anatase fine particles) under photoirradiation at wavelengths longer than 350 nm as a where r is the reaction rate, a the constant, λ the wavelength, and I is the light intensity. The shape of the action spectrum is similar to that of the absorption one and does not present any other new peaks, indicating that the photo-reaction underwent an only photocatalysis mechanism in the whole wavelength range.

The spectra were rather simple; S-doped TiO₂ loaded with or without Fe₂O₃ nanoparticles and P-25 exhibited comparable photocatalytic activities in the UV region. The lower activity level of S-doped TiO₂ loaded with or without Fe₂O₃ nanoparticles may be due to the enhanced recombination of photoexcited electrons and holes in this region, since dopants also acted as a recombination center. A slight shorter-wavelength shift of the spectra of S-doped TiO₂ is also attributable to the enhanced recombination in the near band-gap wavelength.

The action spectrum of S-doped TiO₂ loaded with Fe₂O₃ nanoparticles was further compared with that of P-25 and that of S-doped TiO₂ without loading of Fe₂O₃ nanoparticles. As shown in Fig. 5, all of these three photocatalysts exhibit comparable photocatalytic activities in the UV region. In the visible region, both of the doped TiO₂ photocatalysts show an appreciable VIS response and negligible activity is observed for P-25. The photocatalytic activity level of S-doped TiO₂ loaded with Fe₂O₃ nanoparticles in the visible region is about two-times higher than that of S-doped TiO₂ without loading of Fe₂O₃ nanoparticles. However, its visible response range is not extended and is still maintained at ca. 400–550 nm.

3.4. Photocatalytic decomposition of acetaldehyde on S-doped and N-doped TiO₂ in gas phase

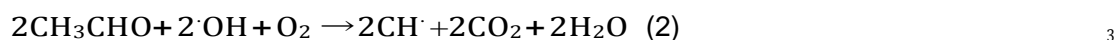
Fig. 6 shows photocatalytic evolution of CO₂ as a result of decomposition of aldehyde on S-doped and N-doped TiO₂ and pure TiO₂ (ST-01, anatase fine particles) under photoirradiation at wavelengths longer than 350 nm as a function of irradiation time. Photocatalytic activities of S-doped and N-doped TiO₂ were similar to that of pure TiO₂ under photoirradiation at wavelengths longer than 350 nm. Despite the enhancement of recombination of photoexcited electrons and holes by doping treatments as described above, total photocatalytic activities of S-doped and N-doped TiO₂ are thought to recover by improvement of photocatalytic activity in the visible light region because pure TiO₂ does not show any photocatalytic activity under visible light.

The activity level for photocatalytic evolution of CO₂ from acetaldehyde on S-doped TiO₂ remained high under visible light irradiation at wavelengths longer than 420 nm, while there was no activity of pure TiO₂ for decomposition of acetaldehyde as shown in Fig. 7. Although photocatalytic activity levels of S-doped TiO₂ were not so high, photocatalytic decomposition of acetaldehyde also proceeded on S-doped TiO₂ under photoirradiation at wavelengths longer than 470 nm. The rate of photodecomposition of acetaldehyde on S-doped TiO₂ decreased rapidly with increase in the wavelength of incident light. These results suggested that apparent quantum efficiency for decomposition of acetaldehyde on S-doped TiO₂ under visible light is much lower than that under UV light.

3.5. Photocatalytic decomposition of acetaldehyde on S-doped and N-doped TiO₂ loaded with or without Fe₂O₃ nanoparticles in gas phase

Fig. 8 shows photocatalytic evolution of CO₂ generated by decomposition of acetaldehyde on S-doped and N-doped TiO₂ loaded with Fe₂O₃ nanoparticles and pure TiO₂ as a function of irradiation time. Photocatalytic activity levels of S-doped and N-doped TiO₂ loaded with Fe₂O₃ nanoparticles are higher than that of pure TiO₂ at the initial stage under photoirradiation at wavelengths longer than 350 nm. However, rates of evolution of CO₂ on both S- and N-doped TiO₂ loaded with Fe₂O₃ nanoparticles slowed down at a certain irradiation time as shown in Fig. 8. Acetic acid and formic acid were mainly generated as intermediates as a result of oxidation of acetaldehyde on doped TiO₂ photocatalysts [50]. CO₂ was evolved from acetaldehyde by oxidation of acetic acid and formic acid on TiO₂ photocatalysts under photoirradiation [50]. The rate of evolution of CO₂ generated by oxidation of formic acid may be different from that of CO₂ generated by oxidation of acetic acid [50]. Therefore, time profiles of evolution of CO₂ on S- and N-doped TiO₂ loaded with Fe₂O₃ nanoparticles are influenced by the compositions of these two processes and their decomposition rates. In order to evaluate the reaction rates of acetic acid and formic acid on N-doped TiO₂ loaded with Fe₂O₃ nanoparticles, photodecomposition of these two compounds on N-doped TiO₂ loaded with Fe₂O₃ nanoparticles, the amount of which was 1 wt%, was examined. The results are shown in Fig. 9A. The reaction rate for decomposition of formic acid is much faster than that of acetic acid on N-doped TiO₂ loaded with Fe₂O₃ nanoparticles. These results suggested that faster reaction at the initial stage for degradation of acetaldehyde is due to degradation of formic acid and that slower reaction at a later stage is due to degradation of acetaldehyde. The starting time of the later stage is consistent with the time of disappearance of acetaldehyde as shown in Fig. 9A. Therefore, both formic acid and acetic acid were generated photocatalytically at an appropriate ratio, and preferential oxidation of formic acid is thought to proceed at the initial stage because oxidation of formic acid occurs more easily than that of acetic acid as described above. The proportion of acetic acid at the later stage is much larger than that at the initial stage. Consequently, acetic acid generated as a result of oxidation of acetaldehyde was mainly oxidized at the later stage. As shown in Fig. 9A, the reaction rate of degradation of acetaldehyde approximately corresponded with that of oxidation of formic acid at the initial stage and the reaction rate of oxidation of acetic acid corresponded with that at the later stage when N-doped TiO₂ loaded with Fe₂O₃ nanoparticles (1.0 wt%) was used. Fig. 10 shows FT-IR spectra of N-doped TiO₂ loaded with Fe₂O₃ nanoparticles after 0.5 and 2.0 h of photoirradiation. Two peaks assigned to acetic acid were observed after photoirradiation for 0.5 and 2.0 h. As discussed above, acetic acid is more stable than formic acid on doped TiO₂ under photoirradiation. Therefore, formic acid might disappear very quickly under photoirradiation because formic acid is easily oxidized.

The reaction rates for degradation of both formic acid and acetic acid gradually decreased with increase in amounts of Fe₂O₃ nanoparticles loaded on N-doped TiO₂ as shown in Fig. 9B. The later stage for oxidation of acetaldehyde on N-doped TiO₂ loaded with Fe₂O₃ nanoparticles, which is due to oxidation of acetic acid, gradually decreased with increase in the amount of Fe₂O₃ nanoparticles loaded on N-doped TiO₂. However, increase in the reaction rate at a faster initial stage, which is due to oxidation of formic acid, was observed with increase in the amount of Fe₂O₃ nanoparticles. Nimlos et al. reported another reaction scheme for oxidation of acetaldehyde on TiO₂ photocatalysts [51]. CO₂ was directly evolved by the reaction between acetaldehyde and OH radicals generated photocatalytically [51]. According to a previous literature [51], we assumed to take place two pathway reactions. First way acetaldehyde was directly oxidized to CO₂ (2). On the other hand, CO₂ was evolved by oxidation of acetaldehyde via acetic acid (3) and (4).



Although the reason for the discrepancies in the rates of the initial stage for degradation of acetaldehyde and oxidation of formic acid using N-doped TiO₂ loaded with a large amount of Fe₂O₃ nanoparticles is not clear, the possibility of direct evolution from acetaldehyde, reported by Nimlos et al., can not be ruled out in our system.

The decrease in the reaction rate of the later stage can be explained as follows. When an excess amount of Fe₂O₃ nanoparticles was loaded on the doped TiO₂ particles, aggregation of Fe₂O₃ nanoparticles easily proceeded [52]. Therefore, photoexcited electrons are accumulated in the aggregates of Fe₂O₃ nanoparticles loaded on the surface of the doped TiO₂. In these circumstances, photogenerated holes disappear easily as a result of the recombination of holes and electrons accumulated in Fe₂O₃ nanoparticles. Improvement in the reaction rate for degradation of acetaldehyde on S-doped and N-doped TiO₂ loaded with Fe₂O₃ nanoparticles is dominated by dispersibility and amount of Fe₂O₃ nanoparticles. Consequently, an excess amount of Fe₂O₃ nanoparticles loaded on S-doped and N-doped TiO₂ shows a low rate constant for degradation of acetaldehyde.

Three compounds, acetaldehyde, formic acid and acetic acid, are included in the initial stage of the reaction.

The presence of these three compounds at the initial stage might be due to the improvement of the reaction rate when an excess amount of Fe₂O₃ nanoparticles was loaded on doped TiO₂. On the other hand, acetic acid is the main component at the later stage of the reaction. Therefore, the reaction rate for oxidation of acetic acid is consistent with the reaction rate of the later stage. As described above, the main factor responsible for improving the reaction rate at the initial stage is not clear yet. Therefore, further investigation is needed to clarify the main factor responsible for the discrepancies between the reaction rate at the initial stage and for oxidation of formic acid. We are now carrying out such investigation.

Photocatalytic activity level of S-doped TiO₂ loaded with Fe₂O₃ nanoparticles was higher than that of S-doped TiO₂ under VIS light irradiation at wavelengths longer than 420 nm as shown in Fig. 11. As discussed in Section 3.3, apparent quantum efficiency of S-doped TiO₂ loaded with Fe₂O₃ nanoparticles was markedly improved compared to that of S-doped TiO₂ without loading of Fe₂O₃ nanoparticles under photoirradiation in the visible light region. We estimated the overall expected gain in efficiency using the solar spectrum. The intensity ratio of UV light and visible light in solar spectrum is 0.06:1. The amount of evolved CO₂ based on this ratio was 157 ppm at 360 min under solar beam as a light source.

4. Conclusions

S-doped and N-doped TiO₂ loaded with Fe₂O₃ nanoparticles have been prepared. Their photocatalytic activities are controlled by changing the amount of Fe₂O₃ nanoparticles loaded on S-doped and N-doped TiO₂. Action spectra of S-doped TiO₂ photocatalyst for oxidation of acetic acid clearly exhibited photocatalytic activity in the visible light region. The photocatalytic activities of S-doped and N-doped TiO₂ for oxidation of acetic acid were improved by loading with Fe₂O₃ nanoparticles on the doped TiO₂. The reaction mechanism of photo-oxidation of acetaldehyde on S-doped and N-doped TiO₂ loaded with or without Fe₂O₃ nanoparticles was discussed. These investigations revealed that acetic acid and formic acid might be generated as intermediates during photocatalytic reactions.

Acknowledgements

This work was supported by a Grant-in-Aid for Scientific Research from the Ministry of Education, Culture, Science, and Technology (MEXT), Japan and Nissan Science Foundation.

- [1] Bahnemann, Chem. Rev. 95 (1995) 69.
- [2] A. Fujishima, T.N. Rao, D.A. Truk, J. Photochem. Photobiol. C: Photochem. Rev. 1 (2000) 1.
- [3] A. Fujishima, K. Honda, Nature 238 (1972) 5551.
- [4] L. Cao, F. Spiess, A. Huang, S.L. Suib, T.N. Obee, S.O. Hay, J.D. Freihaut, J. Phys. Chem. 103 (1999) 2912.
- [5] E.J. Wolfrum, J. Huang, D.M. Blake, P.C. Maness, Z. Huang, J. Fiest, W.A. Jacoby, Environ. Sci. Technol. 36 (2002) 3412.
- [6] J. Theurich, D.W. Bahnemann, R. Vogel, F.E. Dhamed, G. Alhakimi, I. Rajab, Res. Chem. Intermed. 23 (1997) 247.
- [7] S. Yanagida, Y. Ishimaru, Y. Miyake, T. Shiragami, C. Pac, K. Hashimoto, T. Sakata, J. Phys. Chem. 93 (1989) 2576.
- [8] B. Ohtani, J. Kawaguchi, M. Kozawa, S. Nishimoto, T. Inui, J. Chem. Soc., Faraday Trans. 91 (1995) 1103.
- [9] T. Ohno, T. Kigoshi, K. Nakabeta, M. Matsumura, Chem. Lett. (1998) 877.
- [10] T. Ohno, K. Nakabeya, M. Matsumura, J. Catal. 176 (1998) 76.
- [11] F. Soana, M. Sturini, L. Cermenati, A. Albini, J. Chem. Soc., Perkin Trans. 2 (2000) 699.
- [12] R.W. Mattews, J. Chem. Soc., Faraday Trans. 1 80 (1984) 457.
- [13] M. Fujihira, Y. Satoh, T. Osa, Nature 293 (1981) 206.
- [14] M. Dusi, C.A. Muller, T. Mallat, A. Baiker, Chem. Commun. 2 (1999) 197.
- [15] T. Ohno, K. Tokieda, S. Higashida, M. Matsumura, Appl. Catal. A 6462 (2003) 1.
- [16] T. Ohno, T. Mitsui, M. Matsumura, J. Photochem. Photobiol. A 160 (2003) 3.
- [17] M. Anpo, Y. Ichihashi, M. Takauchi, H. Yamashita, Res. Chem. Intermed. 24 (1998) 143.
- [18] M. Anpo, Catal. Surv. Jpn. 1 (1997) 169.
- [19] K. Yamaguchi, S. Sato, J. Chem. Soc., Faraday Trans. 81 (1985) 1237.
- [20] A. Kudo, K. Domen, K. Maruya, T. Ohnishi, Chem. Phys. Lett. 113 (1987) 517.
- [21] K. Sayama, H. Arakawa, J. Photochem. Photobiol. A 94 (1996) 67.
- [22] K. Domen, A. Kudo, T. Ohnishi, N. Kosugi, H. Kuroda, J. Phys. Chem. 90 (1986) 292.
- [23] J.M. Lehn, J.P. Sauvage, R. Sissel, L. Hilaire, Isr. J. Chem. 22 (1982) 168.
- [24] Y. Sakata, T. Yamamoto, T. Okazaki, H. Imamura, S. Tsuchiya, Chem. Lett. 1998 (1998) 1253.

- [25] H. Kato, A. Kudo, *J. Phys. Chem. B.* 106 (2002) 5029.
- [26] T. Ishii, H. Kato, A. Kudo, *J. Photochem. Photobiol. A* 163 (2004) 181.
- [27] T. Ohno, F. Tanigawa, K. Fujihara, S. Izumi, M. Matsumura, *J. Photochem. Photobiol. A* 127 (1999) 107.
- [28] A.K. Ghosh, H.P. Maruska, *J. Electrochem. Soc.* 98 (1994) 13669.
- [29] W. Choi, A. Termin, M.R. Hoffmann, *J. Phys. Chem.* 98 (1997) 13669.
- [30] R.G. Breckenridge, W.R. Hosler, *Phys. Rev.* 91 (1953) 793.
- [31] D.C. Cronmeyer, *Phys. Rev.* 113 (1957) 1222.
- [32] T. Ohno, Y. Masaki, S. Hirayama, M. Matsumura, *J. Catal.* 204 (2001) 163.

- [33] S. Ikeda, C. Abe, T. Torimoto, B. Ohtani, *Electrochemistry* 70 (2002) 442.
- [34] R. Asahi, T. Morikawa, T. Ohwaki, K. Aoki, Y. Taga, *Science* 293 (2001) 269.
- [35] T. Umebayashi, T. Yamaki, H. Ito, K. Asai, *Appl. Phys. Lett.* 81 (2002) 454.
- [36] S.U.M. Khan, M. Al-Shahry, W.B. Ingler Jr., *Science* 297 (2002) 2243.
- [37] M. Anpo, M. Takeuchi, *J. Catal.* 216 (2003) 505.
- [38] A. Fuerte, M.D. Hernández-Alonso, A.J. Maira, A. Martínez-Arias, M. Fernández-García, J.C. Conesa, J. Soria, G. Munuera, *J. Catal.* 212 (2002) 1.
- [39] T. Ohno, T. Mitsui, M. Matsumura, *Chem. Lett* 32 (2003) 364.
- [40] T. Ohno, M. Akiyoshi, T. Umebayashi, K. Asai, T. Mitsui, M. Matsumura, *Appl. Catal. A: Gen.* 265 (2004) 115.
- [41] T. Ohno, T. Tsubota, M. Toyofuku, R. Inaba, *Catal. Lett.* 98 (2004) 255.
- [42] T. Ohno, Z. Miyamoto, K. Nishijima, H. Kanemitsu, F. Xueyuan, *Appl. Catal. A: Gen.* 302 (2006) 62.
- [43] M. Horio, *Nihon Gak. Kyo. Hokoku* 12 (1937) 204.
- [44] R.W. Matthews, *Water Res.* 25 (1991) 1169.
- [45] A. Mills, J. Wang, *J. Photochem. Photobiol. A: Chem.* 127 (1999) 123.
- [46] Y. Nosaka, M. Matsushita, J. Nishino, A.Y. Nosaka, *Sci. Technol. Adv. Mater.* 6 (2005) 1468.
- [47] A.A. Khaleel, *Chem. Dur. J.* 10 (2004) 925.
- [48] H. Stanjek, *Clay Miner.* 37 (2002) 629.
- [49] T. Nakanishi, H. Iida, T. Osaka, *Chem. Lett.* 32 (2003) 1166.
- [50] D.S. Muggli, J.T. MacCue, J.L. Falconer, *J. Catal.* 173 (1998) 470.
- [51] M.R. Nimlos, E.J. Wolfrum, M.K. Brewer, J.A. Fennell, G. Bintner, *Environ. Sci. Technol.* 30 (1996) 3102.
- [52] T. Ohno, *Sulphuric Acid Ind.* 59 (10) (2006) 157.